LIMNOLOGY
and
OCEANOGRAPHY

ASLO

Limnol. Oceanogr. 9999, 2018, 1–18

doi: 10.1002/lno.11067

Biogeography of zooplankton feeding strategy

A. E. Friederike Prowe [1,2*] **André W. Visser,** [2] **Ken H. Andersen,** [2] **Sanae Chiba,** [3,4] **Thomas Kiørboe** [2]

[1]GEOMAR Helmholtz Centre for Ocean Research Kiel, Kiel, Germany
[2]Centre for Ocean Life, National Institute of Aquatic Resources, Technical University of Denmark, Kgs. Lyngby, Denmark
[3]JAMSTEC, Yokohama Institute for Earth Sciences, Yokohama City, Kanagawa, Japan
[4]UNEP-WCMC, Cambridge, UK

Abstract

The trait-based approach is increasingly used in plankton ecology to understand diversity, community dynamics, and biogeography. While on the global scale phytoplankton traits are fairly well established, zooplankton traits are only beginning to be understood. One taxa-transcending aspect of zooplankton diversity is the distinction between ambush and active feeding strategies. We present a global-scale empirical estimate of feeding strategy derived from copepod abundance observations, which for the first time suggests a distinct trait biogeography with ambush feeding as the dominant feeding strategy at higher, but not at lower latitudes. To explain this trait biogeography, we develop a minimalist trade-off based model of feeding strategies based on encounter rates between zooplankton predators and their phyto- and zooplankton prey. Encounter rates are governed by the two traits, size and motility, that trade off against predation risk. Coupled to a three-dimensional dynamic green ocean model, our idealized encounter model captures the observed feeding strategy biogeography. In the model, this pattern arises from competing dominant food chains within the food web and is shaped by a trophic trait cascade of active vs. passive feeding in adjacent trophic levels. The dominant feeding strategy structures the pathways and efficiency of energy and biomass transfer through the model food web, with consequences for primary production, export and higher trophic levels. Understanding feeding strategies is therefore important for fisheries, biogeochemical cycling, and long-term predictions of ecosystem dynamics and functioning by global dynamic green ocean models.

Plankton community structure is one of the key unknowns when attempting to understand ocean ecosystem dynamics and carbon fluxes (Steinberg and Landry 2017). One approach to describing community structure and plankton diversity, and eventually capture it in ecosystem models is the trait-based approach (Litchman and Klausmeier 2008). Transferred from terrestrial ecology first to phytoplankton, it aims to characterize a community in terms of traits rather than taxonomy, and to identify trade-offs between those traits which shape community composition (Litchman et al. 2007). More recently, the trait-based approach has been extended to zooplankton (Litchman et al. 2013) and trait databases have been established for copepods as one of the most common zooplankton groups (Barton et al. 2013; Brun et al. 2017). One important application of these databases is to understand the global biogeography of traits.

For copepods, perhaps the best studied group of zooplankton, the biogeography of various traits has been investigated on the global scale (Brun et al. 2016). While some traits like body size show a clear biogeography featuring a latitudinal gradient, Brun et al. (2016) failed to show any consistent global pattern in feeding strategy. Here, we revisit the issue of the biogeography of copepod feeding strategy. Feeding strategy is one of the central zooplankton traits, linking the key life-task factors of resource acquisition, metabolic costs, and predation risk via clear mechanistic trade-offs (Kiørboe 2011). Feeding modes can be defined by motility on a scale from passive ambush feeding representing a sit-and-wait strategy with low costs and predation risk, to active feeding modes like cruising, which is energetically more costly and increases conspicuousness to predators (Kiørboe et al. 2014). Organisms may thus choose between the low-cost, low-risk, and low-profit passive strategy of ambush feeding and high-cost, high-risk, and high-profit active strategies like cruise or current feeding. Feeding strategies have been found to structure

*Correspondence: fprowe@geomar.de

Additional Supporting Information may be found in the online version of this article.

seasonal plankton community composition through a trophic trait cascade where adjacent trophic levels exhibit alternating strategies (Mariani et al. 2013; Kenitz et al. 2017). Feeding strategies of mesozooplankton are furthermore of significance for ecosystem functions like the transfer of energy and biomass to higher trophic levels. Assuming different trophic interactions between micro- and mesozooplankton changes estimates of phytoplankton-mediated carbon export from 0% to 25% of the primary production (PP; Steinberg and Landry 2017). For such carbon budgets as well as for fisheries production, the trophic position of mesozooplankton, shaped by its trophic interactions, remains a key unknown.

Global biogeochemical models are widely used to budget carbon fluxes and estimate effects of rising concentrations of atmospheric carbon dioxide on oceanic ecosystems and their role in mitigating or amplifying the responses (Bopp et al. 2013). In these models, zooplankton formulations play a pivotal role as dynamic mortality on phytoplankton, which influences simulated ecosystem dynamics and ecosystem functions like PP and the export of carbon to the ocean interior (Anderson et al. 2013; Sailley et al. 2015; Le Quéré et al. 2016). Moreover, predicted changes in PP (Bopp et al. 2013) may be amplified through higher trophic levels (Stock et al. 2014*a*) with consequences for fisheries and the biological carbon pump (Chust et al. 2014; Stock et al. 2017). While a fair amount of attention has been given to resolving the diverse phytoplankton community with its differential resource uses (e.g., Follows and Dutkiewicz 2011; Le Quéré et al. 2016), zooplankton formulations are typically oversimplified (Mitra et al. 2014*a*) and resolve zooplankton trophic interactions in the most basic way. In order to improve our understanding of the role of ocean ecosystems for carbon fluxes and biogeochemistry, global patterns of zooplankton traits and trophic interactions need to be better understood.

Given the relevance of the zooplankton feeding strategy for both ecology and ecosystem functioning and its hypothesized role in shaping seasonal succession, it is striking that no clear biogeography could be identified on the global scale (Brun et al. 2016). In this study, we derive an observational estimate of feeding strategy, focusing on copepods as one of the best studied mesozooplankton groups, and indeed demonstrate a distinct global biogeography of zooplankton feeding strategy. We make use of the fact that on the global scale, ambush feeding is almost entirely confined to the ubiquitous genus *Oithona*. As *Oithona* spp. feed mainly on other zooplankton (Paffenhöfer 1993) and represent a higher trophic level than more herbivorous active feeders (Castellani et al. 2008), their dominance affects food chain length and trophic transfer efficiency, while being important food organisms for fish (*see* Turner 2004 and references therein). In order to examine potential biogeographical patterns, we formulate a minimalistic trade-off based model of feeding strategies and apply it in a global ocean biogeochemical model. We use these simulations in conjunction with observations to understand the trait dynamics and their sensitivity in different regions, and address consequences for predictions of the community structure, trophic level, and net community production (NCP).

Methods

Observations

In order to establish a biogeography of copepod feeding strategy, we focus on the ratio between ambushing and total copepods. This ratio, termed the ambusher fraction, can be estimated from observations as the ratio between the ubiquitous genus *Oithona* as obligate ambushers (Brun et al. 2017) to total copepods. Other facultative ambushing copepod genera like *Centropages* and *Acartia* are abundant mostly in coastal regions and are therefore not considered. The remaining dominant pelagic copepod genera can be considered active feeders (Brun et al. 2017).

We estimate the ambusher fraction from abundance data available from the NMFS-COPEPOD global plankton database (http://www.st.nmfs.noaa.gov/copepod; downloaded November 2017), the Southern Ocean CPR data (Hosie 1999, updated 2015, obtained in January 2015) and the Odate collection (Odate 1994, updated 2002, obtained in January 2016). For each tow where *Oithona* spp. were identified, their abundance fraction of total copepod abundance is calculated. From all data available, we select only tows with abundance measurements of whole animals, identification to at least genus level, and more than one taxon identified, thereby arriving at a total of 46,686 tows. We use abundance fraction rather than biomass fraction (Brun et al. 2017) (1) because of the greater data availability and (2) to avoid hiding the ambusher signal in the observations, as *Oithona* spp. are notably smaller, typically undersampled and thus have lower biomass for similar abundance levels than many actively feeding copepod genera.

Given the heterogeneity of data from different origins, a statistical analysis of the compiled data of the top 200 m is applied to identify which factors differing between the samples may systematically bias the calculated ambusher fraction. We test for the effects of the total number of taxa identified for each tow, the (log-transformed) total abundance of copepods in each tow, latitude, and season. For the latter, we construct an index giving days since peak summer to be able to analyze data from both hemispheres together. A potential sampling bias is corrected for by weighing the observations according to their spatial density. We assume the observed ambusher fraction to be beta distributed and run a general additive model. This analysis complements the model simulations by providing an understanding of what determines the balance between copepod feeding strategies in nature. More details are given in Supporting Information S1.

The model

The trade-off based encounter model

The trait/trade-off-based plankton model is aimed to be as simple as possible in order to allow tractability of structural and parameter sensitivities. A minimalist food web is resolved

by distinguishing the extremes of two trait axes, size, and motility. Motility distinguishes feeding strategy as either motionless ambush feeding, where animals adopt a "sit and wait" strategy and rely on the activity of their prey for encounters, or active feeding, where encounters are facilitated by actively moving or creating a feeding current (Kiørboe 2011). Ambushers are thus restricted to motile prey, while cruisers are assumed to feed on both motile and immotile prey. For simplicity, in the following active feeding will be referred to as "cruise feeding" without intending to exclude other active feeding modes (Kiørboe 2011). The model further distinguishes between two size classes of zooplankton, small (**z**, i.e., microzooplankton) and large (**Z**, i.e., mesozooplankton), each comprising ambushers (***a***, ***A***) and cruisers (***c***, ***C***; Fig. 1). Phytoplankton are represented by a single functional type not resolving different size classes to allow tractability of the model dynamics.

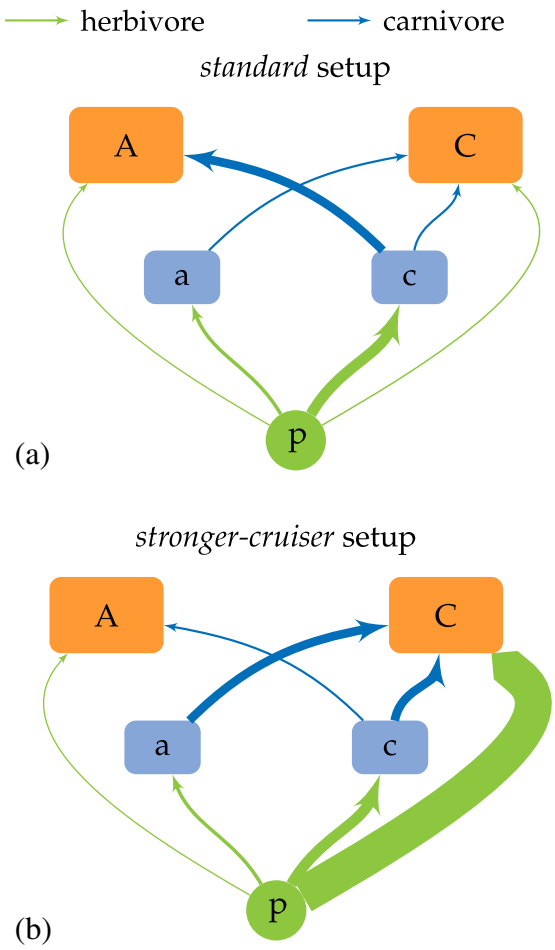

Fig. 1. The *standard* encounter model (**a**) with one phytoplankton type **p** and four zooplankton types characterized by size and feeding strategy: **a** —small ambushers; **c** —small cruisers; **A** —large ambushers; **C** —large cruisers. Line thickness is proportional to the specific encounter rate kernels (β^*). In the *stronger-cruiser* setup (**b**), the food chains related to **C** are strengthened compared to the *standard* setup. [Color figure can be viewed at wileyonlinelibrary.com]

The dynamics for zooplankton k preying on phytoplankton and zooplankton prey $i = \boldsymbol{p}, \boldsymbol{a}, \boldsymbol{c}$ and being preyed upon by zooplankton $l = \boldsymbol{A}, \boldsymbol{C}$ are given by the following equations:

$$k = \boldsymbol{a}, \boldsymbol{c}: \quad \frac{\partial z_k}{\partial t} = \text{ingestion} - \text{predation} - \text{mortality}$$
$$= f_z(T)\ \epsilon_k \sum_i [I_{ik} z_k] - \sum_l [f_Z(T)\ I_{kl} Z_l] - m_k^{\text{lin}} z_k - m_k^{\text{quad}} z_k^2 \quad (1)$$

$$k = \mathbf{A}, \mathbf{C}: \quad \frac{\partial Z_k}{\partial t} = \text{ingestion} - \text{mortality}$$
$$= f_Z(T)\ \epsilon_k \sum_i [I_{ik} Z_k] - m_k^{\text{lin}} Z_k - m_k^{\text{quad}} Z_k^2 \quad (2)$$

with the temperature function $f(T)$, the growth efficiency ϵ, and the linear and quadratic mortality rates m^{lin} and m^{quad}, respectively. Ingestion rates (I in d^{-1}) are calculated as a type 2 functional response

$$I_{ik} = \frac{\beta_{ik}^* \mathcal{P}_{\theta i}}{1 + \sum_i \left[\tau_k \beta_{ik}^* \mathcal{P}_{\theta i}\right]}, \quad (3)$$

based on the predator mass-specific encounter kernel (β^*_{ik} in $\text{m}^3\ \text{mmol P}^{-1}\ \text{d}^{-1}$) with prey concentration $\mathcal{P}_\theta$ including a threshold formulation (Eq. S7 in the Supporting Information S3) and the processing time per biomass (τ) reflecting time for both handling (short) and digestion of prey independent of prey type

$$\tau_k = \frac{1}{I_k^{\max}}. \quad (4)$$

The value of τ_k is derived from observed maximum ingestion rates ($I^{\max}$; Hansen et al. 1997).

For each combination of predator and prey, β^* is calculated based on a mechanistic encounter formulation taking into account swimming speed, detection area, size selectivity, and escape responses (Eq. S5 in the Supporting Information S3), with the underlying parameter values scaling with body size. Ambush and cruise feeding trade off lower or higher encounter rates with lower and higher predation risk and metabolic costs (Visser 2007). As ambush feeders rely on the movement of the prey to elicit encounters, with prey organisms usually smaller (Hansen et al. 1994) and therefore swimming slower (Kiørboe 2011), encounter rates for ambushing predators are on the one hand assumed to be significantly smaller than those for cruising predators. On the other, for cruisers only a small fraction of prey encounters leads to ingestion as their motion may elicit escape responses of the prey (Jakobsen 2001; Kiørboe et al. 2010). The resulting values of β^* (Table 1) determine the balance of interaction strengths in the model as indicated by the line thickness in Fig. 1. This configuration of encounter kernels sets up two different dominant food chains for **A** and **C**, where **A** relies on **c** and **C** relies on **p** as main prey. Details on the parameterization including the temperature function are given in the Supporting Information S3.

Table 1. Predator mass-specific encounter kernels $\beta^{\#}$ (m^3 mmol P^{-1} d^{-1}) between predators (columns) and their prey (rows).

predator PFT	*a*	c	A		C	
prey PFT		*z* (*no-strategy*)†	*standard*	*stronger-cruiser* ‡	*standard*	*stronger-cruiser*‡
p	30.79	96.30	0.26	**0.65**	12.98	**324.48**
a	—	—	—	—	19.24	**76.98**
c	—	—	76.98	**19.24**	19.34	**77.36**

#Values of $\beta^* = \beta / w$ are calculated from Eq. S5 in the Supporting Information by normalizing with predator mass *w*.
†In the *no-strategy* setup, both **z** PFTs use the values indicated for **c**.
‡β^* values changed in the *stronger-cruiser* configuration with feeding interactions of **C** enhanced are printed in bold.

The three-dimensional ecosystem model

We use the Massachusetts Institute of Technology general circulation model (MITgcm) coupled to a reduced version of the "Darwin" ecosystem module (Follows et al. 2007; Dutkiewicz et al. 2009, 2013) including the encounter model described above. The ecosystem module version comprises the original prognostic equations for three nutrients (phosphorus, nitrogen, and iron), dissolved and particulate organic matter, while only one (small) phytoplankton type and four zooplankton types (two small, two large) are implemented. Phosphorus is used as the main currency of the model. Temperature-dependent phytoplankton growth takes into account limitation by light, including effects of self-shading, and by a Liebig-type limitation by the most limiting nutrient according to a Michaelis-Menten formulation. The phytoplankton parameters are chosen to represent an average small type in Dutkiewicz et al. (2009). Phytoplankton losses include a linear mortality, sinking, and zooplankton predation according to the equations given in Supporting Information S3. The export of organic matter to depth occurs mainly via particulate organic matter produced by phytoplankton mortality, sloppy feeding, and zooplankton egestion and mortality. Sinking of phytoplankton is not considered.

The physical model is forced offline by the ECCO-GODAE state estimates (Wunsch and Heimbach 2007). The coupled ecosystem-circulation model is integrated on a global grid of 1° resolution with 24 depth levels for 10 yr, by which time it displays a repeating annual cycle in nutrients, plankton concentrations, and PP. The *standard* model simulation employs the encounter model as described above.

Model dynamics may be sensitive to two kinds of changes concerning the plankton food web: first, modifying the strength of the trade-off between feeding strategies without changing the trophic network configuration as detailed in Fig. 1a, and second, changing the configuration and strength of trophic interactions in that these influence how complex a community is resolved by the model. The trade-off strength can be modified, e.g., by increasing (decreasing) the linear mortality of large cruisers or ambushers to make a strategy more (less) risky. The balance of trophic interactions changes when the values of the encounter kernels β^* change relative to each other.

Model sensitivity is examined in simulations analogous to the *standard* model runs but with three alternative configurations:

1. *low-/high-cruiser-mortality*: increased and decreased linear mortality for **C**.
   These configurations represent the simplest way to change the trade-off strength in the model, as **C** is able to utilize all food sources in the model.
2. *stronger-cruiser*: with increased feeding by large cruisers (**C**) on phytoplankton, small ambushers and small cruisers (**p**–**C**, **a**–**C**, **c**–**C**).
   This configuration directly changes encounter kernel values, and thereby the balance of trophic interactions, for the focus group, large zooplankton, relative to each other (Fig. 1; Table 1).
3. *no-strategy*: feeding strategies omitted for **z** (all **z** are **c**).
   This configuration indirectly changes trophic interaction balance by removing a distinction in prey types on the small zooplankton level, thereby reducing trophic diversity.

The underlying parameter changes are given in Table 1 and in Supporting Information Tables S2, S3.

For comparison with the observed ambusher fraction, we calculate the simulated ambusher fraction as ratio of large ambushers to total large zooplankton (**A**/[**A**+**C**]). As both **A** and **C** have the same body weight, values calculated from the biomass-based model output represent an abundance-based measure of the ambusher fraction.

Model assessment

Observations on the global scale that may serve to evaluate our model results are generally scarce because categorization according to feeding strategies and motility requires species resolution. In addition to the ambusher fraction, we used meso- and microzooplankton biomass data without distinction of feeding strategy available from the MAREDAT data set (Moriarty and O'Brien 2013) and from the compilation by

Buitenhuis et al. (2010) to compare to total simulated large and small zooplankton. Observational biomass was converted to model units of mmol P m^{-3} using a molar C : P ratio of 100. Observations of phytoplankton biomass were taken from the MAREDAT database. We use the sum of observed picophytoplankton, coccolithophore, *Phaeocystis* spp., diazotroph, and diatom biomass (Buitenhuis et al. 2012; Leblanc et al. 2012; Luo et al. 2012; Vogt et al. 2012; O'Brien et al. 2013), likewise converted to model units, as the model does not distinguish different phytoplankton types and the one phytoplankton type is not outcompeted by other types. Simulated biomass may therefore underestimate observed values.

Estimates of phytoplankton net primary production (NPP) are available from satellite data of ocean color (e.g., Behrenfeld and Falkowski 1997; Uitz et al. 2010), but are associated with substantial uncertainties (Saba et al. 2011). More accurate in situ measurements of NPP are available, albeit with very limited spatial coverage. We used the compilation of in situ NPP presented by Buitenhuis et al. (2013) in conjunction with the satellite-based estimate of Behrenfeld and Falkowski (1997) for comparison with simulated phytoplankton PP.

Results

Observed feeding strategy biogeography

The most striking feature in the observed ambusher fraction of total copepod abundance is the latitudinal pattern from low values at low latitudes to highest values at high latitudes (Fig. 2). Poleward of about 40° latitude values span the entire range from complete dominance of cruisers (**C**) to complete dominance of ambushers (**A**; *Oithona* spp.; Fig. 2c). Equatorward of 40°, the ambusher fraction is consistently below 0.4. The large spread is easily understood given the heterogeneity of the observations encompassing different sampling methods, depths, times, and taxonomic resolution in addition to various types of ocean ecosystems. Furthermore, latitudes exhibiting a large range of *Oithona* spp. dominance are those where seasonality is a prevailing factor. The statistical analysis confirms latitude as the dominating factor affecting the ambusher fraction (*see* Supporting Information S1 for further details). In this respect, our results contrast the study by Brun et al. (2016) which could not identify any latitudinal gradient in copepod feeding strategy (*see* "Discussion" section).

Model plausibility

Before presenting the simulated biogeography of feeding strategies, we compare the *standard* configuration of the model to available observations of zooplankton and phytoplankton. Simulated **Z** biomass is generally within the range of the observations and reflects the latitudinal pattern (Fig. 3). The model tends to underestimate coastal and shelf zooplankton biomass likely because of the comparatively low-grid resolution in these more dynamic areas of the ocean. It reproduces general biogeographical patterns with higher biomass in western boundary currents, upwelling regions and the subtropical front boundary of the Southern Ocean, even though the model does not reproduce well the observed high values in the polar seas. Considering that the model uses just one phytoplankton functional group and resolves neither differential nutrient use for phytoplankton nor seasonal vertical migration for mesozooplankton, the simulation of the mesozooplankton compartment in terms of biogeography is reasonable.

For microzooplankton, a meaningful comparison is limited by the scarcity and the large spread of the data. Again, the simulated **z** biomass lies within the (wide) range of the observations and generally captures the biogeography with higher and lower values in high and low latitudes, respectively. Elevated biomass at low latitudes, as also seen for mesozooplankton biomass, is not captured by the model. The lack of microzooplankton biomass here likely reflects the low-phytoplankton biomass (Fig. 4) and PP (Fig. 5) simulated in these latitudes.

Simulated PP and phytoplankton biomass generally underestimate the observations in both the oligotrophic gyres and the coastal and equatorial upwelling regions (Fig. 5). This

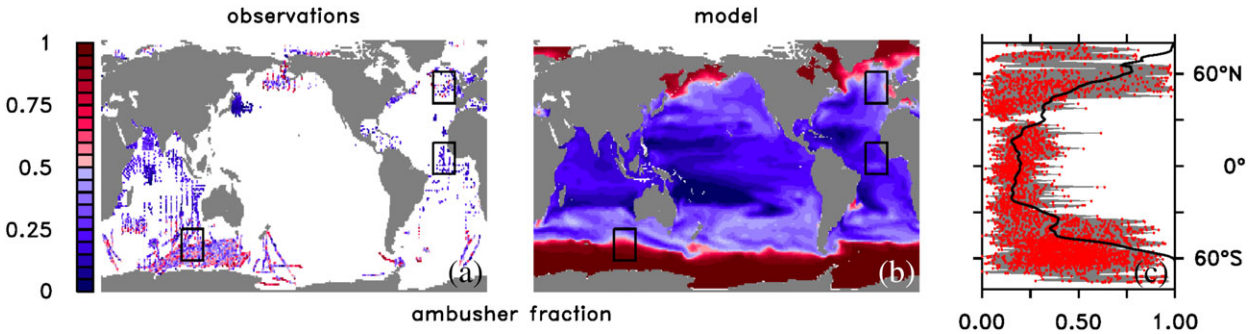

Fig. 2. (**a**) Observed ambusher fraction of total copepods at all stations where *Oithona* spp. as proxy for ambushing copepods was identified. (**b**) Simulated annual average ambusher fraction. (**c**) The zonal average of the simulated ambusher fraction (black line) together with all observational data points shown in panel a (red dots), gray shading indicates the range of observations. All data are averages from 0 m to 100 m depth. Boxes in panels (**a**) and (**b**) indicate the locations examined in Fig. 6.

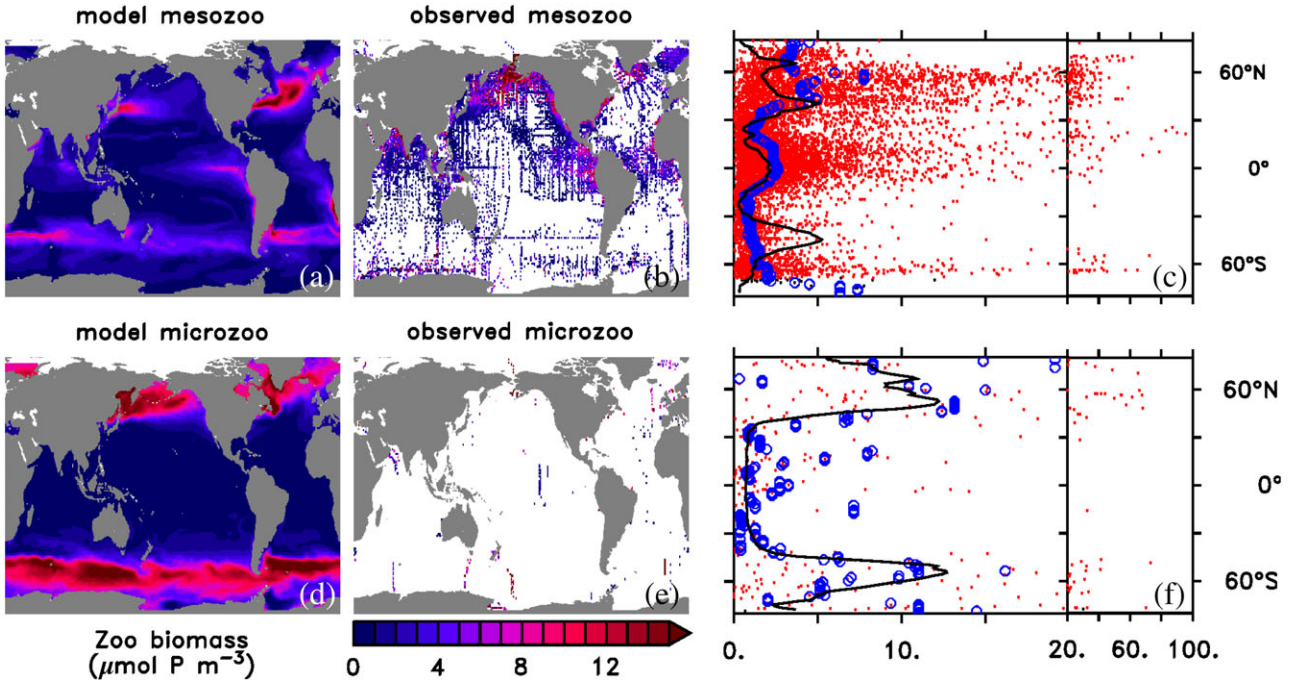

Fig. 3. Simulated annual average (**a, d**) and observed (**b, e**) biomass of mesozooplankton (**a–c**) and microzooplankton (**d–f**) of the *standard* configuration. Individual data points (red) indicate the range of observations with the median (blue circles), in comparison with the zonal median of the model data (black line; **c**, **f**).

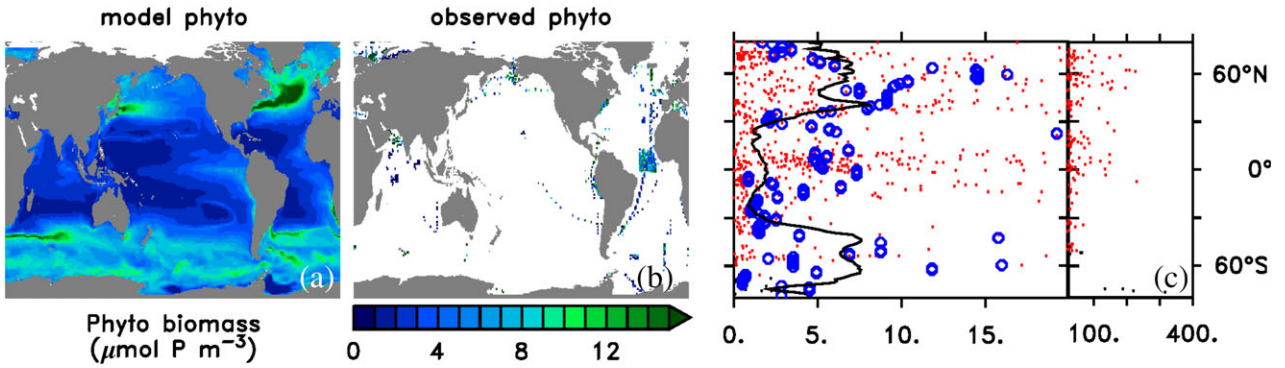

Fig. 4. Simulated annual average (**a**) and observed (**b**) phytoplankton biomass of the *standard* configuration. Individual data points (red) indicate the range of observations with the median (blue circles), in comparison with the zonal median of the model data (black line; **c**).

tendency is known from previous applications of the model configuration providing the basis for our setup (Follows et al. 2007; Prowe et al. 2012*a*), and might partly be caused by the relatively coarse, non-eddy-permitting spatial resolution underestimating vertical transport of nutrients (Clayton et al. 2017). Coarse resolution simulations furthermore tend to overestimate phytoplankton production and biomass in the temperate latitudes, which also occurs in our simulations. Furthermore, higher phytoplankton diversity in models is related to higher PP (Prowe et al. 2012*a*,*b*). Using only one phytoplankton type might therefore also add to underestimating observed PP, although biggest effects are expected in high latitudes (Prowe et al. 2012*b*) where the model overestimates observed PP. Another potential reason for the overestimated difference in PP between subtropics and temperate latitudes may be a poor resolution of the microbial web including the microzooplankton as primary consumers of PP (Schmoker et al. 2013). Trying to adjust community structure in order to improve the PP predictions would mostly compensate biases related to the ocean physics. Moreover, observational estimates are either too sparsely distributed (in the case of ^{14}C PP) or associated with large uncertainties (in case of satellite estimates) to motivate more thorough tuning of the model for the present study.

In any event, tuning biogeochemical ocean models to observations is generally not straight forward (Löptien and

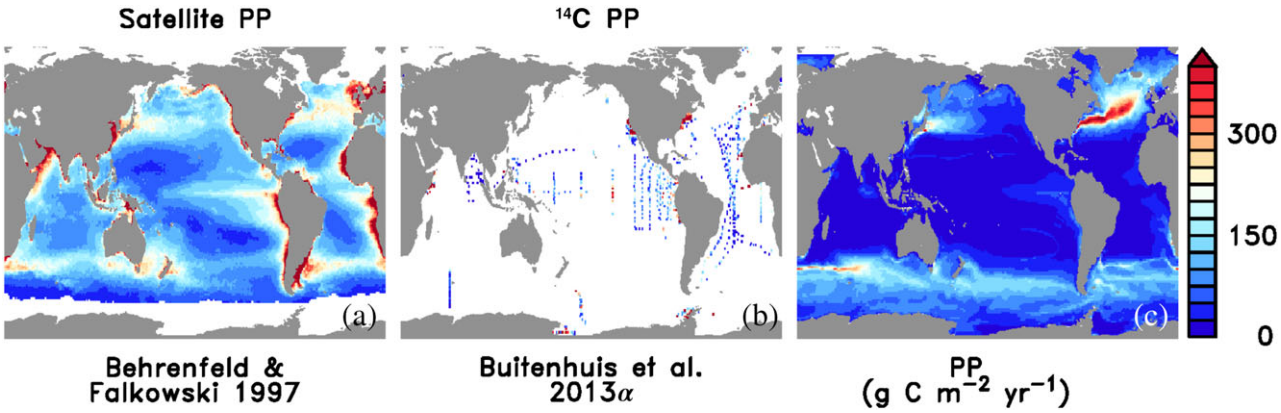

Fig. 5. Observed NPP from satellite observations (**a**) and oceanic measurements of ^{14}C NPP (**b**) compared to PP simulated with the *standard* configuration (**c**).

Dietze 2015). Plankton biomass reflects the balance of source and loss fluxes and may thus be unaffected if both are adjusted simultaneously. Hence, simulated PP rates may be tuned to any level as long as loss terms are changed accordingly. The focus of this study is not on simulating quantitatively ecosystem functions related to PP like oceanic carbon uptake, but to investigate the biogeography of feeding strategies and its potential effects on such ecosystem functions. For this purpose, the model provides spatial patterns of plankton biomass and PP in sufficient agreement to observations. We therefore refrain from extended tuning of this highly simplified model and focus on general mechanisms underlying the results.

Simulated feeding strategy biogeography

The *standard* simulation captures the latitudinal gradient observed for the ambusher fraction (Fig. 2b). Highest annual average ambusher fraction near one indicates a low abundance of cruisers in the Southern Ocean and the polar oceans. Intermediate values indicating a nearly balanced abundance of **A** and **C** in the annual average are predicted in the temperate productive regions and the upwelling regions in the eastern boundary currents. Lowest prevalence of **A** is found in the oligotrophic gyres. The underlying biomass concentrations of each zooplankton type are shown in Supporting Information Fig. S4.

This pattern results from the distinction of feeding strategies and the related trade-off between low cost, risk, and profit ambush feeding and high cost, risk, and profit cruise feeding employed for both small and large zooplankton. It reflects the two contrasting food chains for **A** and **C** with their preferred prey **c** and **p**, respectively. The mechanisms at play are best revealed when examining specific locations (Fig. 2) representing different biogeographical regimes underlying the observed trait biogeography. These regimes are shaped by latitudinal environmental gradients and ocean circulation. In terms of latitudinal gradients, the existence of a seasonal cycle in the temperate to polar latitudes is the most prominent characteristic. Regarding ocean circulation, regions are set apart by seasonal mixing or the degree of upwelling of nutrients, distinguishing productive from oligotrophic regimes. In order to approach an understanding of differences between the provinces, as a first indication Fig. 6 shows observations for example regions from high, temperate, and oligotrophic low latitudes with comparatively good seasonal data coverage.

In oligotrophic regions with low productivity, shown here for a location in the tropical Atlantic (Fig. 6a,d,g,j), environmental conditions are expected to be mostly uniform throughout the year and the ambusher fraction does not show any seasonal variation. As already seen in Fig. 2a, the ambusher fraction here is confined to values below about 0.4. In the model, large cruisers **C** successfully compete with the small zooplankton for phytoplankton **p** as food source (Fig. 7j), and thereby relieve small ambushers **a** from strong top-down control (Fig. 7a). Small cruisers **c**, however, are top-down controlled as main prey for **A** (Fig. 7d,g) given the low **p** biomass and productivity (Fig. 8a). Small ambushers **a** can thus thrive throughout the year and come to dominate the small zooplankton **z**. Higher prevalence of **c** during the first half of the year occurs at one to two orders of magnitude lower abundance than **a**, not compromising the dominance of **C**. In consequence, **C** relies on an efficient **p**-**C** food chain, while **A** is food limited by their preferred prey **c**. In the annual average, this is seen in the low-ambusher fraction in the lower latitudes, with lowest values in the strongly oligotrophic subtropical gyres (Fig. 2).

In the temperate latitudes with higher annual average PP, exemplified for the eastern North Atlantic (Fig. 6b,e,h,k), both food chains operate in parallel, leading to a more balanced coexistence of **C** and **A** and an intermediate ambusher fraction. The monthly observations suggest higher ambusher fraction during winter. However, data coverage in this season is very sparse at this particular location and does not allow any solid conclusion about seasonality. The on average low-ambusher fraction again reflects an efficient **p**-**C** food chain

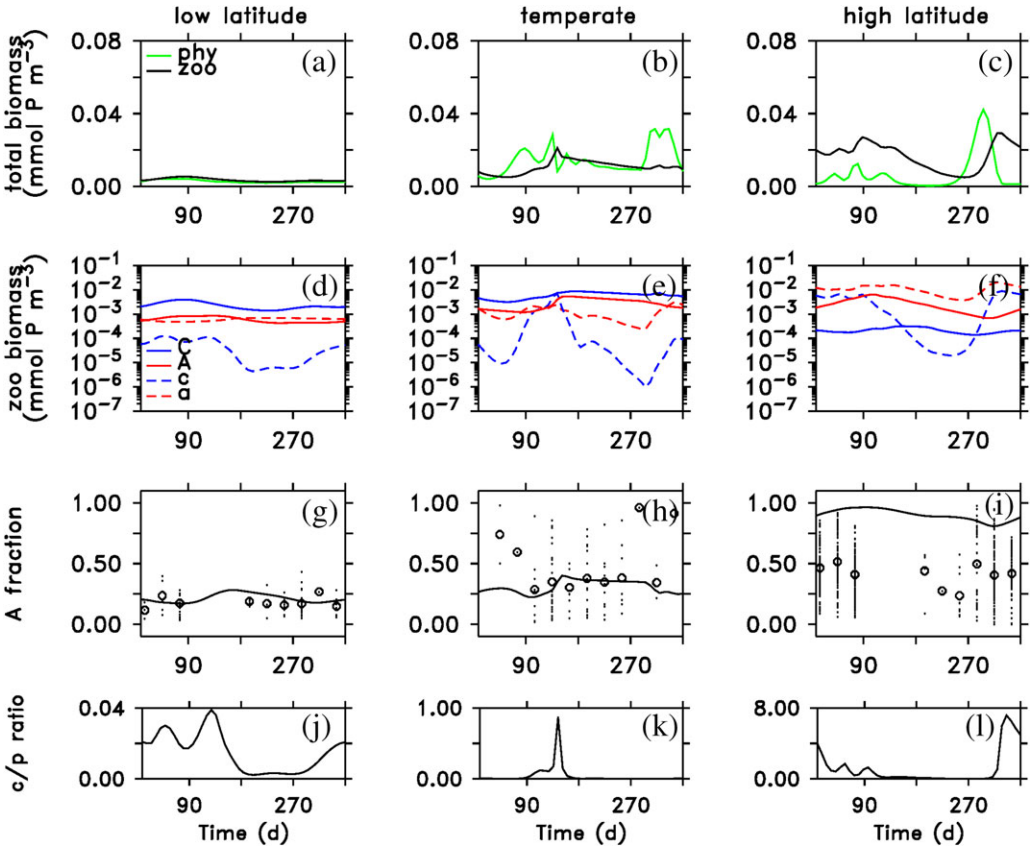

Fig. 6. Simulated seasonal dynamics in the top 100 m of (**a–c**) total phytoplankton and zooplankton biomass; (**d–f**) zooplankton community composition of large and small ambushers and cruisers; (**g–i**) ambusher fraction; and (**j–l**) simulated ratio of small cruiser to small phytoplankton biomass in low (right panels), temperate (center panels) and high latitudes (right panels); observed ambusher fraction values (dots; circles: monthly average) comprise all values from the respective regions indicated in Fig. 2 with simulated results located at the center of the boxes. [Color figure can be viewed at wileyonlinelibrary.com]

throughout the year (Figs. 7k, 8b). **C** loses its competitive advantage over **c** only during the spring bloom (Fig. 7e), when PP is highest. The seasonality in the ambusher fraction ultimately reflects a change in the dominance of the different small zooplankton types (**c** vs. **a**) throughout the season. In spring, **c** comes to dominate by making use of the **p** bloom, but is soon top-down controlled by **A** as best competitor for **c** (Fig. 7e,h). **a** then dominates in the less productive summer and winter times. This leads to a higher fraction of **A** following the spring bloom. These dynamics yield the intermediate annual average values predicted throughout the temperate latitudes (Fig. 2). Variations in timing, length of the productive season, and so forth may explain the large range seen in the observations.

In high latitudes with seasonally varying productivity and food availability like the Southern Ocean near Antarctica (Fig. 6c,f,i,l), the observations suggest a more equal contribution of ambushers and cruisers. In the model, in contrast to the other regions, **A** dominates over **C** because **C** cannot compete against **c** for **p** as prey. This effect results from the different temperature functions used in the model (Supporting Information Fig. S5). Ingestion rates for **C**, though generally lower, increase with temperature more strongly than for **c**. The competitive advantage of **c** over **C** through higher encounter kernels β^* for prey **p** thus decreases in colder regions. With an average annual temperature of 4.2°C, **c** has a 50 times higher β^* and 6.5 times higher maximum ingestion rate than **C** compared to factors 25 and 3.5, respectively, for 24°C at the low-latitude location (Supporting Information Fig. S5e). In consequence, **C** sustains themselves via the less efficient **p**-**a**-**C** food chain and **A** outcompetes **C** (Fig. 8c), leading to a high-ambusher fraction. A useful proxy indicating the dominant food chain in this model is the ratio of **c** to **p** biomass. While **c**/**p** is high at the high-latitude location, it is notably lower at both temperate and low-latitude locations (Fig. 6j–l). Removing the differential temperature sensitivity of small and large zooplankton and assuming a common temperature dependence for all plankton functional types (PFTs) decreases the ambusher fraction at this location to intermediate levels in better agreement with the observations (simulation not shown), but values agree less well with the observations in subtropical regions. A better fit to the

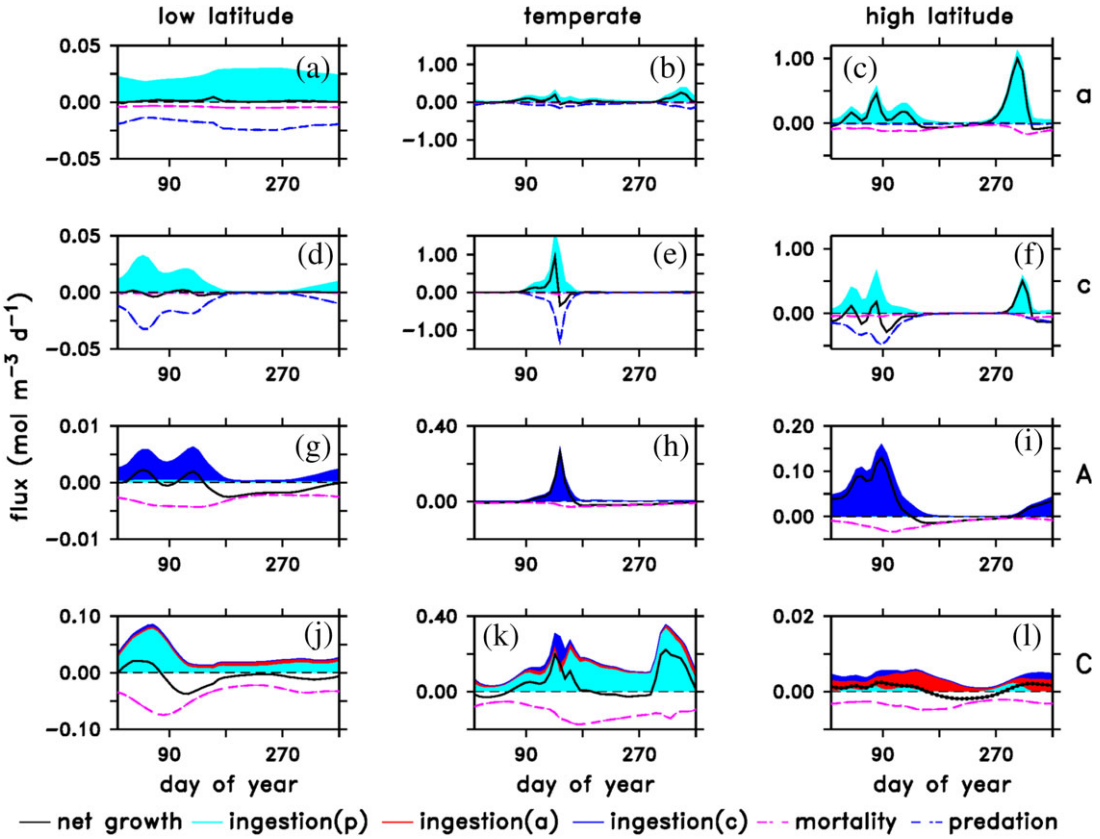

Fig. 7. Simulated seasonal dynamics of net growth, ingestion, mortality, and predation fluxes in the top 100 m of the different zooplankton types: small ambushers (**a–c**), small cruisers (**d–f**), large ambushers (**g–i**) and large cruisers (**j–l**). Dynamics are shown for the same locations in the low (left panels), temperate (center panels), and high (right panels) latitudes as used in Fig. 6.

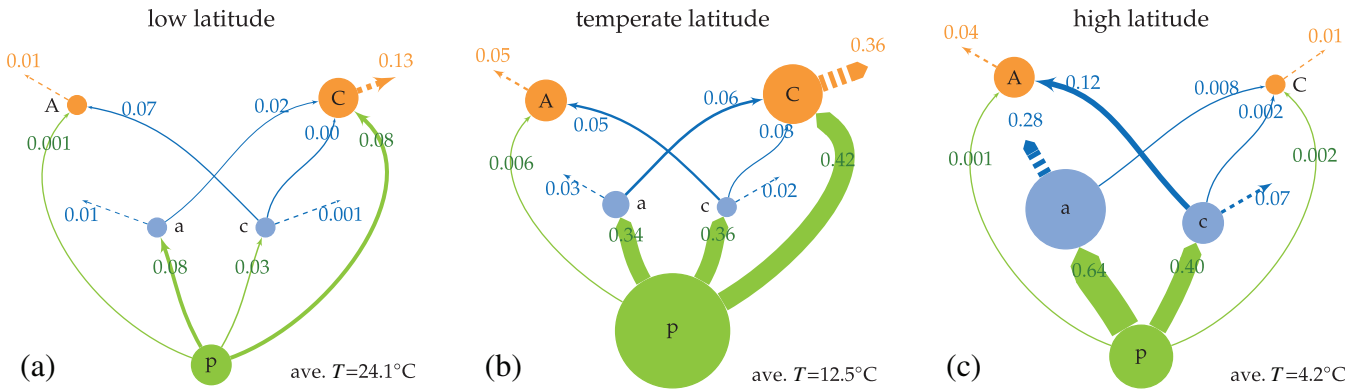

Fig. 8. Annual budget of biomass and fluxes within the model food web comprising phytoplankton (**p**), small ambushers (**a**) and cruisers (**c**), and large ambushers (**A**) and cruisers (**C**) at the same locations in low (**a**), temperate (**b**), and high (**c**) latitudes as used in Fig. 6. Circle area is scaled to integrated biomass, line thickness is scaled to integrated fluxes of ingestion (solid arrows) and mortality (dashed arrows). [Color figure can be viewed at wileyonlinelibrary.com]

observations can also be obtained by lowering loss terms like the linear mortality for **C**, thereby weakening the trade-off between risks and profits in the model. Selected changes in feeding interaction strengths and other parameters are used in the following section to give an impression of model sensitivity and identify factors potentially affecting the foraging strategy.

In summary, the model suggests that different prey spectra accessible to ambushers and cruisers drive different competing pathways through the food web. With competitive advantages sensitive to temperature, these food chains give rise to the biogeographical pattern of feeding strategies observed for copepods.

Model sensitivity

In the following, we use different modifications to the *standard* model to gauge the sensitivity of the hypothesized mechanism for explaining the observations. As described in the methods section, the trade-off strength is modified by changing the linear mortality of **C** in the *low-/high-cruiser-mortality* simulations. The balance of trophic interactions is changed directly from that in the *standard* run in the *stronger-cruiser* simulation (Table 1), and indirectly via a reduction of trophic diversity by omitting feeding strategies for small zooplankton in the *no-strategy* simulation. The model's sensitivity is assessed in terms of (1) the emergent community structure as expressed by the ambusher fraction (Fig. 9), (2) the trophic level of large zooplankton (**A** + **C**; Fig. 10), and (3) net community productivity (Fig. 11).

Ambusher fraction

The strength of the ambush-cruise feeding trade-off is easily changed by increasing or decreasing the linear mortality for **C**. Higher mortality makes active cruise feeding even riskier compared to passive ambush feeding, thereby moving the competitive advantage from **C** toward **A**. As a result, **A** comes to dominate to a larger degree at lower latitudes (Fig. 9a). The opposing effect, an extended latitudinal range of **C**, occurs when lowering the mortality for **C**. The changes in **C** dominance with lower mortality also affect the adjacent lower trophic level of small zooplankton, with notably reduced dominance of **a** in temperate latitudes (Fig. 9b). In the case of linear mortality, parameter changes only affect the level of the ambusher fraction and thereby the latitudinal range, but the shape of the latitudinal gradient appears largely robust.

The balance of trophic interactions is the central difference between the *standard* and the *stronger-cruiser* setups (Fig. 1; Table 1). The *standard* setup distributes interaction strengths in a somewhat balanced way allowing for dominance of both **A** and **C** at different locations (Figs. 2, 9) and times (Fig. 6). When more advantages are given to **C** in the *stronger-cruiser* setup by increasing their feeding encounters, thereby strengthening the **p**-**C** food chain, **C** come to outcompete **A** at all latitudes except the southernmost polar regions. This simulation thus approaches a configuration without feeding strategies for large zooplankton. The opposite effect, a strong dominance of **A** at all latitudes, may be expected when shifting the advantage toward **A**. This can be done as above by changing parameters affecting the interaction strength. Alternatively, **A** also receive more profit when their preferred prey, **c**, increases. The *no-strategy* configuration, which omits feeding strategies for **z** and resolves only **c**, thus leads to the expected dominance of **A** across all latitudes. This setup almost removes the latitudinal pattern of the ambusher fraction. A similar tendency, e.g., enhanced **A** dominance in mid-latitudes, is also found for other parameter changes affecting the trophic interaction strengths (not shown).

In summary, model sensitivity in terms of the ambusher fraction is tightly linked to the interaction strengths, and thereby the representation of the plankton community formulated in the model. Parameter changes not affecting the configuration of interaction strengths but the strength of the ambusher-cruiser trade-off, like **z** mortality, control the latitudinal range where a given feeding strategy dominates.

Trophic level

The trophic level of the large zooplankton **Z** (TL_Z) is a powerful indicator summarizing the pathways of energy and biomass realized in the model. It is furthermore a proxy for an important ecosystem function, because a higher trophic level of large zooplankton corresponds to a lower efficiency of the transfer of PP to higher trophic levels such as fish. The simulated TL_Z is calculated by summing ingestion on one prey type relative to the total ingestion of a given predator, where ingestion of phytoplankton is weighted with a factor 1 ($TL_p = 1$) and ingestion of small zooplankton is weighted with a factor 2 ($TL_z = 2$). For total large zooplankton **Z**,

$$TL_Z = 1 + TL_p \cdot \frac{I_{pA} + I_{pC}}{\sum_i [I_{iA} + I_{iC}]} + TL_z \cdot \frac{I_{cA} + I_{aC} + I_{cC}}{\sum_i [I_{iA} + I_{iC}]}. \quad (5)$$

where, e.g., I_{pA} is ingestion of **p** by **A** and $\sum_i[I_{iA} + I_{iC}]$ is total ingestion of both **A** and **C** on all types of prey *i*.

Generally, the latitudinal pattern of TL_Z is similar across simulations with higher TL_Z (lower efficiency) in polar regions and the subtropical oligotrophic gyres (10°–30° latitude), and

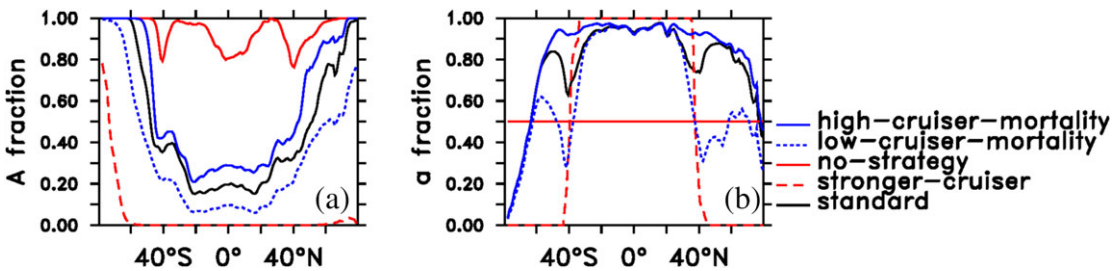

Fig. 9. Simulated zonal annual average fraction ambusher fraction for large (**a**) and small (**b**) zooplankton types (0–100 m) for the standard *standard* run (black) and configurations listed in the "Methods" section. [Color figure can be viewed at wileyonlinelibrary.com]

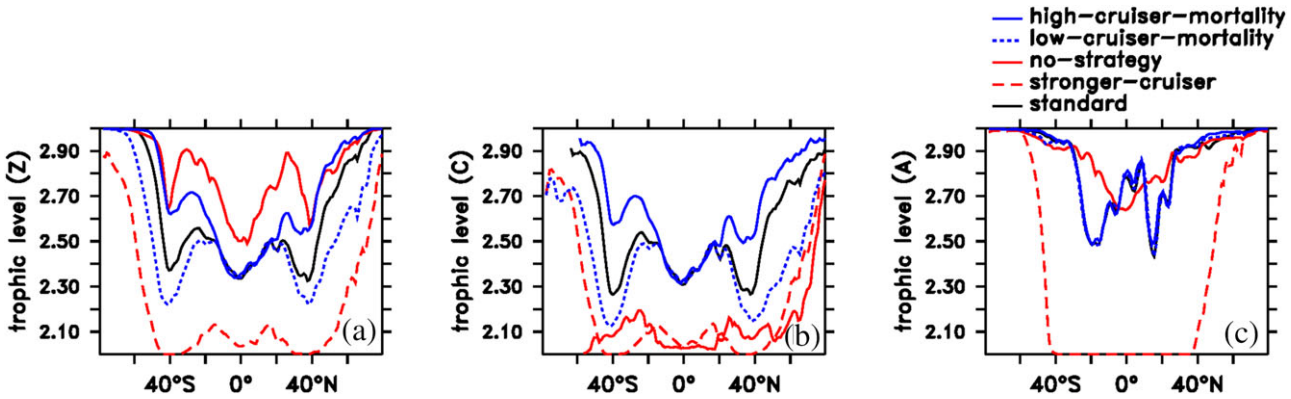

Fig. 10. Zonal average trophic level of large zooplankton (**Z** ; **a**), comprising cruisers (**C** ; **b**), and ambushers (**A** ; **c**) in the top 0–100 m for the standard *standard* run (black) and configurations listed in the "Methods" section. [Color figure can be viewed at wileyonlinelibrary.com]

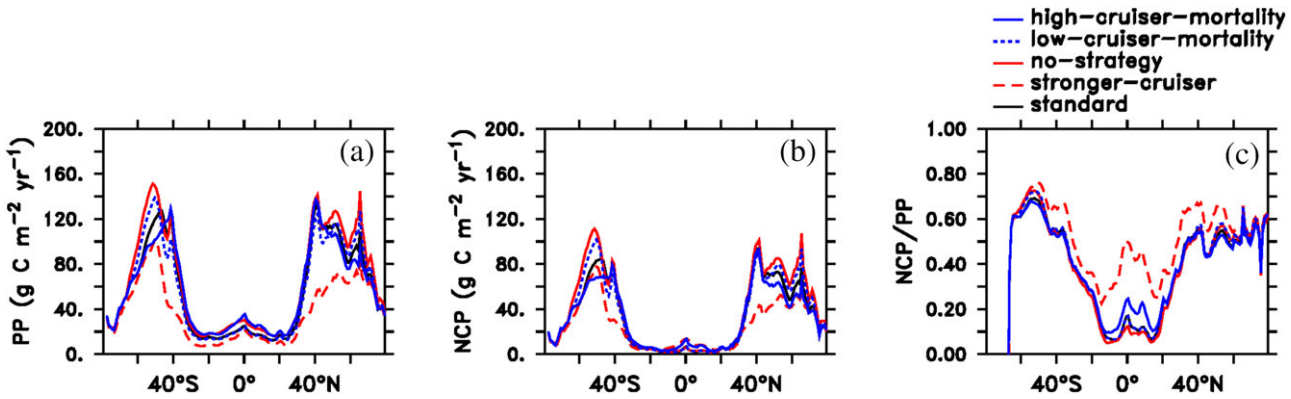

Fig. 11. Zonal average PP (**a**), NCP (**b**) and the ratio of NPP to PP (**c**) in the top 0–100 m for the standard *standard* run (black) and configurations listed in the "Methods" section. [Color figure can be viewed at wileyonlinelibrary.com]

low TL_Z (higher efficiency) in the productive western boundary currents (40° latitude) and low-latitude upwelling regions. The strength of the latitudinal gradient differs substantially between model configurations (Fig. 10a).

The *standard* simulation predicts an intermediate TL_Z around 2.5 with herbivory (TL_Z = 2) more pronounced in productive latitudes. Carnivory (TL_Z = 3) is more important in the latitudes representing the oligotrophic gyres and becomes the dominant feeding mode in high latitudes. Changes in the trade-off strength, as produced by changing the mortality of **C**, have a weak effect on the TL_Z and hence on the energy flows through the ecosystem. With cruise feeding being riskier, **C** switch from herbivory to a more carnivorous diet. The higher mortality of **C** only leads to an increase of the trophic level of **C** (TL_C; Fig. 10b), but does not affect the trophic level of **A** (TL_A; Fig. 10c).

The largest variation is seen between the configurations affecting the trophic interaction strengths directly, i.e., the *standard*, *stronger-cruiser*, and *no-strategy* configurations. Promoting **C** feeding on **p** in the *stronger-cruiser* simulation yields a TL_Z near 2 (pure herbivory) except for the Southern Ocean and the subpolar Northern latitudes. Highest overall TL_Z is reached when **A** feeding is promoted by assuming only motile small zooplankton (**z**=**c**). In contrast to changes in trade-off strength, changing trophic interactions affects the trophic levels of both **A** and **C**. Promoting **C** feeding in the *stronger-cruiser* setup decreases its TL from a balanced mixed diet to almost pure herbivory outside of subpolar/polar latitudes (Fig. 10b). Ambushers can only persist at high latitudes (Fig. 9) relying on an increasing degree of carnivory toward the poles (Fig. 10c). Promoting **A** feeding in the *no-strategy* setup instead increases the TL_A, while **C** persist on **p** only.

In summary, the trophic level of large zooplankton is particularly sensitive when modifying trophic interactions, and integrates both biomass and feeding mode changes. For adjustments of the trade-off strength between ambush and cruise feeding through mortality changes, the TL_Z reflects only a change in diet of **C**, resulting in smaller changes of the TL_Z. Here, the change in competition does not lead to a diet change in **A**. Despite all changes in trophic level, the latitudinal structure is conserved across all simulations: the TL of **Z** is notably lower in relatively more productive latitude bands of the equatorial upwelling and western boundary currents (around 40° latitude).

Primary and net community production

Different trophic pathways may influence other ecosystem functions simulated by the model. As further examples we calculate PP and NCP. NCP is calculated as NCP = PP − community respiration, with community respiration in the model represented by (bacterial) degradation of organic matter, since zooplankton respiration is not resolved explicitly. NCP is an upper estimate of the fraction of PP available for export into the deep ocean.

All configurations simulate a similar pattern of ocean productivity (Fig. 11) with higher PP and NCP in temperate latitudes due to the western boundary currents (Fig. 5), low values in the subtropical oligotrophic gyres and elevated production in the equatorial upwelling regions. The largest difference in simulated PP and NCP are found between the *standard* and the *stronger-cruiser* setup (Fig. 11). The *stronger-cruiser* run has markedly lower values than the *standard* run, particularly in the temperate latitudes, thereby underestimating the observational estimates even more. The lower PP coincides with a notably lower ingestion of **p** by **C**, the only zooplankton type with pronounced biomass throughout the year. At the same time, a strong decrease in the TL_C indicates a diet shift from a mixed phyto- and zooplankton diet to almost pure herbivory. In contrast, in the *standard* run, **C**, **A**, and **a** persist throughout the year. **c** appears in both runs only during the spring bloom, a pattern following from the pronounced top-down control. The lower ingestion rate in the *stronger-cruiser* run, in particular combined with the absence of **c**, in turn causes less recycling of nutrients and less recycled production. **Z** production is predominantly channeled into particulate matter which may sink out of the surface ocean instead of dissolved organic matter being recycled within. This larger fraction of PP available for export is reflected in a higher ratio of NCP to PP of 67% in the *stronger-cruiser* compared to 56% in the *standard* simulation. It occurs in the temperate latitudes with seasonal vertical mixing of nutrients into the surface mixed layer. In latitudes dominated by regenerated production, e.g., the subtropics, the difference in PP and NCP between configurations is minimal. In the *no-strategy* setup, PP and NCP both increase by 15%, while in the *stronger-cruiser* setup, PP and NCP decrease by 36% and 24%, respectively. Although productivity decreases overall in the *stronger-cruiser* setup, the model predicts a higher availability of this production for export compared to the other simulations.

Discussion

Observed and simulated biogeography

Our analysis of the observed ambusher fraction of total copepod abundance reveals a striking latitudinal pattern of feeding strategy that is also captured by the model: high-latitude regions are dominated by ambush feeding copepods, while low latitudes exhibit a combination of ambushing and cruise (active) feeding copepods. This pattern is robust to a potential underestimation in net samples (Gallienne and Robins 2001) as ambusher fraction values lie within a confined range at low latitudes, where nets with mesh sizes mostly below 250 μm were used (Supporting Information Fig. S1). Such nets are expected to be more effective in catching *Oithona* spp. than coarser meshed sampling gear typically used in temperate and higher latitudes, where the dominance of *Oithona* spp. is higher.

The feeding mode biogeography reported here contrasts the weak pattern found by Brun et al. (2016). Their analysis was based on the same data from the COPEPOD database used here. However, data from the Southern Ocean and the Odate data set were not included, which in our analysis notably strengthens the pattern in the Southern compared to the Northern hemisphere (Fig. 2). Most importantly, Brun et al. (2016) used observations in terms of biomass which due to the small size of *Oithona* spp. compared to other copepod genera might hide the signal. Our abundance-based analysis increases the signal-to-noise ratio and is thus able to identify a pronounced latitudinal gradient in feeding strategy not evident in Brun et al. (2016).

The trade-off based model employed facilitates an understanding of the feeding mode biogeography by focusing on the most important trade-off related to the feeding mode: profit from ingestion vs. metabolic cost and predation risk. The fact that this one trade-off already yields a pattern similar to the one observed speaks for the explanatory power of the underlying theory. More support for the notion that the trade-off drives the observed latitudinal pattern is provided by it weakening when the trade-off strength is being reduced as shown by the sensitivity analysis. The model dynamics underlying the annual average biogeography reflect the trophic trait cascade identified by Kenitz et al. (2017) using time-series observations at Sta. L4 in the English Channel. Adjacent trophic levels show opposing dominant feeding modes (active vs. passive), giving rise to a seasonal cycle driven ultimately by bottom-up nutrient availability for the primary producers. This mechanism operating temporally at Sta. L4 gives rise to regionally different regimes under different environmental conditions. Through different dominant food chains it produces the distinct biogeography simulated by our global model. Trophic trait cascades are thus seen using two different models, our global one and the local one by Kenitz et al. (2017), with different formulations and underlying modeling approaches but with the same inherent trade-off. This fact again supports the idea that a simple trade-off may explain observed patterns to a large degree independent of methodological details. While for phytoplankton, seasonality of motile and nonmotile types is relatively well documented (e.g., Barton et al. 2013), similar studies for zooplankton are less common (Kenitz et al. 2017) and the seasonality of feeding interactions and related traits is still being established (Mariani et al. 2013; Brun et al. 2017).

In addition to trophic cascades and dominant food chains, the assumed temperature dependence of zooplankton

ingestion plays a considerable role in modifying the underlying pattern. This study employs differential temperature functions for small and large zooplankton (Rose and Caron 2007), which predict a weakening of the competition between these two predator guilds with rising temperatures. The stronger competition in the cold high latitudes intensifies the dominance of ambush over cruise feeding in the model. Different experimental data syntheses (e.g., Eppley 1972; Rose and Caron 2007; Bissinger et al. 2008), however, imply different assumptions about whether predators can keep up with their prey at colder temperatures in particular (Franzé and Lavrentyev 2014). As the outcome of this competition in our model determines the balance of trophic interactions and ultimately ecosystem functions, it is important to analyze model sensitivity to a larger variety of temperature functions in the future.

Limitations

The detailed examination of the seasonal cycle simulated by the model highlights some limitations of the simplified formulations used here. In temperate latitudes, one might expect large active feeders (**C**) to profit from a spring bloom rather than **A** via **c** (Mariani et al. 2013; Kenitz et al. 2017). In the present model, this could potentially be achieved by strengthening the **p**-**C** link as the *stronger-cruiser* simulation does not simulate any ambushers except for at the highest latitudes. In nature, however, one would expect a different trophic pathway: large phytoplankton (often diatoms) dominating the spring bloom would be directly available to **C** (Irigoien et al. 2004; Mariani et al. 2013). In order to capture this succession of phytoplankton types, more phytoplankton size classes and potentially different nutrient requirements like Si for diatoms would need to be resolved. Moreover, while feeding strategies for mesozooplankton like copepods are relatively well established (Kiørboe 2011), for microzooplankton the relevance of active and passive feeding modes is not clear. Here, other trophic interactions like mixotrophy or intraguild predation may play a larger role by widening the energy/prey spectrum (Franzé and Modigh 2013; Mitra 2016).

In the Mauretanian upwelling, the model simulates a stable dominance of **C** throughout the year in apparent good agreement with observations. This good fit is likely to arise for the wrong reasons, though. In the model, the region is oligotrophic and small ambushers **a** with their low-metabolic costs come to dominate the small zooplankton **z**, thereby feeding the **p**-**a**-**C** food chain. In contrast, the observations suggest a substantial amount of PP (Fig. 5), driven by upwelling of nutrient-rich deep waters. This would lead to the **p**-**c**-**A** food chain dominating in the model, or, as discussed above, to a trophic link currently not resolved between large phytoplankton and **C**. In our simulation, the coarse resolution of the model likely hinders the upwelling of nutrients and thereby PP (Clayton et al. 2017).

Regarding seasonality, one of the most striking ecological aspects omitted in the model is the vertical migration of copepods. Vertical migration is observed both on a diurnal basis with organisms commonly located in deeper layers during day than at night as well as seasonally with copepods overwintering at large depths (Ohman and Romagnan 2016; Baumgartner and Tarrant 2017). However, smaller copepods like *Oithona* spp. appear to migrate vertically to a notably lesser degree than other genera. *Oithona* spp. in particular have been found productive in the surface layer of subpolar waters throughout winter at high latitudes while other copepods overwinter in the deep ocean (Zamora-Terol et al. 2013). In the current model, this aspect may explain the overestimated dominance of *Oithona* spp. simulated in the highest latitudes as well as the poor seasonal fit in the temperate locations examined.

Seasonal and diurnal vertical migration might be another mechanisms to explain the observed biogeography of feeding strategies. Cruisers may be assumed to migrate to greater depth in order to reduce their metabolic costs at times of low productivity. For ambushers, this need would be smaller given their lower energy expense for motility (Kiørboe and Hirst 2014). Furthermore, if cruisers migrate out of the euphotic zone during daytimes with high visibility for visual predators, ambushers may seek this refuge to a lesser degree given their less conspicuous behavior (Kiørboe et al. 2010). Consequently, for a considerable fraction of time especially in latitudes with seasonally low productivity, the surface ocean would be dominated by passive feeders, with active feeders hiding at depth (Ohman and Romagnan 2016). This effect is partly captured implicitly by assuming slow growth rates paired with higher mortality for cruisers in the high latitudes, while ambushers can persist throughout the year. Observations with improved temporal (daily and seasonal) and vertical coverage are needed, however, to test this hypothesis.

Another hypothesis that may explain the dominance of ambush feeders—*Oithona* spp. in particular—at high latitudes is related to the diet. *Oithona* spp. are expected to feed on sinking fecal pellets, and have been suggested to at times even constituting a "coprophageous" filter that reduces the vertical flux of fecal pellets of larger calanoids in particular (Gonzalez and Smetacek 1994). Thus, *Oithona* spp. might be abundant where large calanoids are abundant, i.e., in the polar regions (Brun et al. 2016). Both hypotheses require a substantial effort in terms of model development. In particular, vertical migration is only beginning to be resolved in global biogeochemical models (Aumont et al. 2018). Testing these hypotheses thus has to be the subject of future studies.

Food web structure and ecosystem functions

The model limitations described above can be summarized to arise from the rigid nature of both the trophic interactions and the formulations used to reflect the behavior of the organisms. In natural plankton food webs, trophic interactions are very diverse and vary seasonally. They are maybe best described by location-specific food-web models (e.g., D'Alelio et al. 2016). Such models, however, are too complex to be used for predictions on the global scale and simplifying them

is not straight forward. Previous attempts to include some diversity in global models have focused on phytoplankton and employed simplistic trophic interactions (Follows et al. 2007; Prowe et al. 2012*a*). Diverse feeding interactions were implemented either by way of multiple PFTs (e.g., Le Quéré et al. 2016) or in size-based models configured using allometric relationships (Ward et al. 2012, 2013). However, in PFT-type models often the intended food web structure is not the one obtained in the simulations (Sailley et al. 2013). Purely size-structured models which do not take into account other traits may miss important trophic interactions that do not follow a simple size-based prey preference (Su et al. 2018).

Distinguishing feeding strategies for zooplankton as demonstrated here represent another way of including feeding diversity in global models. The *standard* setup yields a balanced contribution of both ambushers and cruisers to the large (i.e., meso)zooplankton. The resulting regional pattern of the trophic levels for large zooplankton (TL_Z) agrees well with other model predictions (Stock et al. 2014*b*): productive regions yield lower TL_Z than less productive regions, in agreement with traditional theory (Ryther 1969). Notably different patterns of TL_Z, implying very different transfer efficiencies of energy and biomass through the food web, are predicted by the *stronger-cruiser* and *no-strategy* configuration with somewhat simpler trophic interactions. Simulations with a diverse mixture of carnivorous and herbivorous feeding interactions seem to coincide with higher PP. While all model setups might be tunable to yield similar values, it is currently not clear which estimates are closest to nature. Observations question to which degree less productive ocean regions have indeed lower trophic transfer efficiencies than productive ones (San Martin et al. 2006), and trophic level estimates based on $\delta^{15}N$ levels are subject to substantial uncertainties (Gutierrez-Rodriguez et al. 2014).

In any case, in the model biomass and production is easily shifted between large ambushers and large cruisers (Fig. 9), and is reflected in a corresponding change in trophic level (Fig. 10). The same signal is seen in both productivity and the export capability of the ecosystem as indicated by the NCP/PP ratio (Fig. 11). The lower TL_Z in the *stronger-cruiser* simulation corresponds to a higher NCP/PP ratio. Thus a similar amount of PP, often used as key variable for comparing model simulations and assessing global change (Bopp et al. 2013), may have very different consequences for higher trophic levels and related ecosystem functions like the production available for fisheries. In particular, the composition of the copepod community may affect juvenile fish abundance (Bi et al. 2011). Our model demonstrates that feeding strategies underlie the key uncertainties in budgeting carbon fluxes through the planktonic ecosystem (Steinberg and Landry 2017), as they provide the mechanistic basis for different trophic pathways, directly or via one or more microzooplankton steps, to the mesozooplankton. This analysis demonstrates a first attempt at resolving feeding strategies explicitly in a global ocean ecosystem model in order to work toward quantifying the effects of trophic interaction variability globally and for biogeochemical questions.

The study adds to other recent work showing that adding diversity in feeding interactions, e.g., in terms of mixotrophy, may enhance ecosystem functions like export to the deep ocean (Ward and Follows 2016). Mixotrophy (Flynn et al. 2013; Mitra 2014*b*) and intraguild predation (Franzé and Modigh 2013) operate mostly on the level of microzooplankton. Model studies of mesocosm experiments highlight the importance of these interactions for the observed dynamics (Larsen et al. 2015; Su et al. 2018). Still, few dynamic ecosystem models to date resolve such processes (e.g., Flynn and Mitra 2009; Ward et al. 2011, 2012; Ward and Follows 2016). Most of these models rely on fixed trophic interactions and are prone to showing a high sensitivity to the exact formulations and parameterizations (Mitra 2014*a*), as seen for the model presented here. Substantial effects of such fixed zooplankton formulations are commonly found in global scale models (Anderson et al. 2010, 2013; Prowe et al. 2012*b*; Hashioka et al. 2013; Sailley et al. 2013; Le Quéré et al. 2016). They comprise aspects from ecology, like stability and coexistence (Cropp et al. 2017), to ecosystem functions, like the carbon export into the sediments/the deep ocean (Anderson et al. 2010, 2013; Sailley et al. 2015; Ward and Follows 2016). Ultimately, it is desirable to find ways to formulate interactions with few parameters in a flexible way that may be applied to the wide range of environmental conditions and prey environments characterizing the global ocean. Optimality-based modeling in combination with trait/trade-off based modeling is a promising approach in this direction (Smith et al. 2011, 2014) and has been applied to the global scale for phytoplankton (Arteaga et al. 2014). For zooplankton, few optimality-based models exist (Pahlow and Prowe 2010; Visser and Fiksen 2013; Marki and Pahlow 2016; Su et al. 2018) and none have been applied globally.

How effects of trophic interaction formulations translate to long-term predictions of global change is currently not clear. It is becoming apparent, however, that predicted PP changes (Bopp 2013) may be amplified across trophic levels depending on food web dynamics (Stock et al. 2014*a*). This trophic amplification can be explained in terms of changes in zooplankton growth efficiency, trophic level and the coupling between zooplankton and phytoplankton. It may in turn cause larger changes in fisheries resources and a reduction in the potential of the biological carbon pump than expected from NPP changes alone (Chust 2014; Stock 2017). The central role of zooplankton in biogeochemical and fisheries models (Mitra 2014*a*) thus underscores the importance of formulating effective flexible descriptions of plankton trophic interactions in global biogeochemical models.

Conclusions

This study presents the first global biogeography of passive vs. active feeding modes observed for copepods. A global

synthesis of abundance observations of the contribution of *Oithona* spp. to total copepod abundance shows a higher fraction in high latitudes and consistently low values in low latitudes. This latitudinal gradient is captured by a simplified model of zooplankton feeding strategies based on mechanistic formulations and trade-offs between encounter rates with prey on the one side and metabolic costs and predation risk on the other. The inherent trade-off provides a first explanation for the global biogeography of passive vs. active feeding modes observed for copepods. The dominance of active or passive feeding strategies is determined by dominance of either herbivorous or carnivorous food chains supporting active and passive feeding, respectively. The resulting ratio of passive to active feeders depends, particularly for cold temperatures in high latitudes, to a substantial degree on which temperature dependence for zooplankton ingestion is used. The ratio of passive to active feeding affects the overall trophic level of zooplankton, which is important for fish production, and leads to different levels of ecosystem functions like primary and NCP.

The model's simplicity allows an in-depth analysis and understanding of the underlying mechanisms on the global scale. At the same time, several limitations of both the ecological and the physical model compromise the realism of the predictions in certain regions. Given the demonstrated sensitivity of the model dynamics to the configuration of trophic interactions, a higher resolution of the phytoplankton community in terms of size and nutrient use strategies, like incorporating diatoms or dinoflagellates, can be expected to affect predictions notably. For such a more complex network of trophic interactions, a structured exploration of model sensitivity to parameter values would be required in order to obtain strong conclusions. Such an in-depth analysis is maybe best performed in zero- or one-dimensional idealized model setups configured to capture representative locations in different biogeochemical provinces. Processes inherent in the physical model like the vertical supply of nutrients may also compromise the realism of the predicted feeding strategy gradient via affecting the identity and productivity of primary producers. Comparing simulations with different vertical nutrient supply in upwelling regions, for example, may further help to understand the dynamics underlying the feeding strategy biogeography.

While all models are wrong (Box 1979), the one presented here reveals the sensitivity of simulated ecosystem functions to rigid trophic interaction formulations. It thus represents a valuable step toward, and motivation for, incorporating flexible and diverse feeding interactions in global biogeochemical models. This process should be the focus of future modeling efforts to determine the role of ecology in global biogeochemical models. Our analysis indicates that trade-off-based models for zooplankton may explain and ultimately help to constrain uncertainties in budgeting carbon fluxes through oceanic food webs.

References

Anderson, T. R., W. C. Gentleman, and B. Sinha. 2010. Influence of grazing formulations on the emergent properties of a complex ecosystem model in a global ocean general circulation model. Prog. Oceanogr. **87**: 201–213. doi:10.1016/j.pocean.2010.06.003

Anderson, T. R., D. O. Hessen, A. Mitra, D. J. Mayor, and A. Yool. 2013. Sensitivity of secondary production and export flux to choice of trophic transfer formulation in marine ecosystem models. J. Mar. Syst. **125**: 41–53. doi:10.1016/j.jmarsys.2012.09.008

Arteaga, L., M. Pahlow, and A. Oschlies. 2014. Global patterns of phytoplankton nutrient and light colimitation inferred from an optimality-based model. Global Biogeochem. Cycles **28**: 648–661. doi:10.1002/2013GB004668

Aumont, O., O. Maury, S. Lefort, and L. Bopp. 2018. Evaluating the potential impacts of the diurnal vertical migration by marine organisms on marine biogeochemistry. Global Biogeochem. Cycles. doi:10.1029/2018GB005886

Barton, A. D., A. J. Pershing, E. Litchman, N. R. Record, K. F. Edwards, Z. V. Finkel, T. Kiørboe, and B. A. Ward. 2013. The biogeography of marine plankton traits. Ecol. Lett. **16**: 522–534. doi:10.1111/ele.12063

Baumgartner, M. F., and A. M. Tarrant. 2017. The physiology and ecology of diapause in marine copepods. Ann. Rev. Mar. Sci. **9**: 387–411. doi:10.1146/annurev-marine-010816-060505

Behrenfeld, M. J., and P. G. Falkowski. 1997. Photosynthetic rates derived from satellite-based chlorophyll concentration. Limnol. Oceanogr. **42**: 1–20. doi:10.4319/lo.1997.42.1.0001

Bi, H., W. T. Peterson, J. Lamb, and E. Casillas. 2011. Copepods and salmon: Characterizing the spatial distribution of juvenile salmon along the Washington and Oregon coast, USA. Fish. Oceanogr. **20**: 125–138. doi:10.1111/j.1365-2419.2011.00573.x

Bissinger, J. E., D. J. S. Montagnes, J. Sharples, and D. Atkinson. 2008. Predicting marine phytoplankton maximum growth rates from temperature: Improving on the Eppley curve using quantile regression. Limnol. Oceanogr. **53**: 487–493. doi:10.4319/lo.2008.53.2.0487

Bopp, L. and others 2013. Multiple stressors of ocean ecosystems in the 21st century: Projections with CMIP5 models. Biogeosci. Discuss. **10**: 3627–3676. doi:10.5194/bgd-10-3627-2013

Box, G. E. P. 1979. Robustness in the strategy of scientific model building, p. 201–236. *In* R. L. Launer and G. N. Wilkinson [eds.], Robustness in statistics. Academic Press.

Brun, P., M. R. Payne, and T. Kiørboe. 2016. Trait biogeography of marine copepods - an analysis across scales. Ecol. Lett. **19**: 1403–1413. doi:10.1111/ele.12688

Brun, P., M. R. Payne, and T. Kiørboe. 2017. A trait database for marine copepods. Earth Sys. Sci. Data **9**: 99–113. doi:10.5194/essd-9-99-2017

Buitenhuis, E. T., R. B. Rivkin, S. Sailley, and L. Quéré. 2010. Biogeochemical fluxes through microzooplankton. Global Biogeochem. Cycles **24**. doi:10.1029/2009GB003601

Buitenhuis, E. T. and others 2012. Picophytoplankton biomass distribution in the global ocean. Earth Sys. Sci. Data **4**: 37–46. doi:10.5194/essd-4-37-2012

Buitenhuis, E. T., T. Hashioka, and C. L. Quéré. 2013. Combined constraints on global ocean primary production using observations and models. Global Biogeochem. Cycles **27**: 847–858. doi:10.1002/gbc.20074

Castellani, C., X. Irigoien, D. J. Mayor, R. P. Harris, and D. Wilson. 2008. Feeding of *Calanus finmarchicus* and *Oithona similis* on microplankton assemblage in the Irminger Sea, North Atlantic. J. Plankton Res. **30**: 1095–1116. doi:10.1093/plankt/fbn074

Chust, G. and others 2014. Biomass changes and trophic amplification of plankton in a warmer ocean. Glob. Chang. Biol. **20**: 2124–2139. doi:10.1111/gcb.12562

Clayton, S., S. Dutkiewicz, O. Jahn, C. Hill, P. Heimbach, and M. J. Follows. 2017. Biogeochemical versus ecological consequences of modeled ocean physics. Biogeosciences **14**: 2877–2889. doi:10.5194/bg-14-2877-2017

Cropp, R., I. Moroz, and J. Norbury. 2017. The role of grazer predation strategies in the dynamics of consumer-resource based ecological models. J. Sea Res. **125**: 34–46. doi:10.1016/j.seares.2017.05.003

D'Alelio, D., S. Libralato, T. Wyatt, and M. R. d'Alcala. 2016. Ecological-network models link diversity, structure and function in the plankton food-web. Sci. Rep. **6**. doi:10.1038/srep21806

Dutkiewicz, S., M. J. Follows, and J. G. Bragg. 2009. Modeling the coupling of ocean ecology and biogeochemistry. Global Biogeochem. Cycles **23**: GB4017. doi:10.1029/2008GB003405

Dutkiewicz, S., J. R. Scott, and M. J. Follows. 2013. Winners and losers: Ecological and biogeochemical changes in a warming ocean. Global Biogeochem. Cycles **27**: 463–477. doi:10.1002/gbc.20042

Eppley, R. W. 1972. Temperature and phytoplankton growth in the sea. Fish. Bull. **70**: 1063–1085.

Flynn, K. J., and A. Mitra. 2009. Building the "perfect beast": Modelling mixotrophic plankton. J. Plankton Res. **31**: 965–992. doi:10.1093/plankt/fbp044

Flynn, K. J., D. K. Stoecker, A. Mitra, J. A. Raven, P. M. Glibert, P. J. Hansen, E. Graneli, and J. M. Burkholder. 2013. Misuse of the phytoplankton-zooplankton dichotomy: The need to assign organisms as mixotrophs within plankton functional types. J. Plankton Res. **35**: 3–11. doi:10.1093/plankt/fbs062

Follows, M. J., S. Dutkiewicz, S. Grant, and S. W. Chisholm. 2007. Emergent biogeography of microbial communities in a model ocean. Science **315**: 1843–1846. doi:10.1126/science.1138544

Follows, M. J., and S. Dutkiewicz. 2011. Modeling diverse communities of marine microbes. Ann. Rev. Mar. Sci. **3**: 427–451. doi:10.1146/annurev-marine-120709-142848

Franzé, G., and M. Modigh. 2013. Experimental evidence for internal predation in microzooplankton communities. Mar. Biol. **160**: 3103–3112. doi:10.1007/s00227-013-2298-1

Franzé, G., and P. J. Lavrentyev. 2014. Microzooplankton growth rates examined across a temperature gradient in the Barents Sea. PLoS One **9**: e86429. doi:10.1371/journal.pone.0086429

Gallienne, C. P., and D. B. Robins. 2001. Is *Oithona* the most important copepod in the world's oceans? J. Plankton Res. **23**: 1421–1432. doi:10.1093/plankt/23.12.1421

Gonzalez, H. E., and V. Smetacek. 1994. The possible role of the cyclopoid copepod *Oithona* in retarding vertical flux of zooplankton fecal material. Mar. Ecol. Prog. Ser. **113**: 233–246. doi:10.3354/meps113233

Gutierrez-Rodriguez, A., M. Decima, B. N. Popp, and M. R. Landry. 2014. Isotopic invisibility of protozoan trophic steps in marine food webs. Limnol. Oceanogr. **59**: 1590–1598. doi:10.4319/lo.2014.59.5.1590

Hansen, B., P. K. Bjørnsen, and P. J. Hansen. 1994. The size ratio between planktonic predators and their prey. Limnol. Oceanogr. **39**: 395–403. doi:10.3354/meps113233

Hansen, P. J., P. K. Bjørnsen, and B. W. Hansen. 1997. Zooplankton grazing and growth: Scaling within the 2-2,000-μm body size range. Limnol. Oceanogr. **42**: 687–704. doi:10.4319/lo.1997.42.4.0687

Hashioka, T. and others 2013. Phytoplankton competition during the spring bloom in four plankton functional type models. Biogeosciences **10**: 6833–6850. doi:10.5194/bg-10-6833-2013

Hosie, G. 1999. Southern Ocean Continuous Zooplankton Records. Australian Antarctic Data Centre - CAASM metadata; [accessed 2015 January]. Available from https://data.aad.gov.au/metadata/records/AADC-00099

Irigoien, X., J. Huisman, and R. Harris. 2004. Global biodiversity patterns of marine phytoplankton and zooplankton. Nature **429**: 863–867. doi:10.1038/nature02593

Jakobsen, H. H. 2001. Escape response of planktonic protists to fluid mechanical signals. Mar. Ecol. Prog. Ser. **214**: 67–78. doi:10.3354/meps214067

Kenitz, K. M., A. W. Visser, P. Mariani, and K. H. Andersen. 2017. Seasonal succession in zooplankton feeding traits reveals trophic trait coupling. Limnol. Oceanogr. **62**: 1184–1197. doi:10.1002/lno.10494

Kiørboe, T. 2011. How zooplankton feed: Mechanisms, traits and trade-offs. Biol. Rev. **86**: 311–339. doi:10.1111/j.1469-185X.2010.00148.x

Kiørboe, T., H. Jiang, and S. P. Colin. 2010. Danger of zooplankton feeding: The fluid signal generated by ambush-

feeding copepods. Proc. R. Soc. Lond. B **277**: 3229–3237. doi:10.1098/rspb.2010.0629

Kiørboe, T., and A. G. Hirst. 2014. Shifts in mass scaling of respiration, feeding, and growth rates across life-form transitions in marine pelagic organisms. Am. Nat. **183**: E118–E130. doi:10.1086/675241

Kiørboe, T., H. Jiang, R. J. Gonçalves, L. T. Nielsen, and N. Wadhwa. 2014. Flow disturbances generated by feeding and swimming zooplankton. Proc. Natl. Acad. Sci. USA **111**: 11738–11743. doi:10.1073/pnas.1405260111

Larsen, A., J. K. Egge, J. C. Nejstgaard, I. Di Capua, R. Thyrhaug, G. Bratbak, and T. F. Thingstad. 2015. Contrasting response to nutrient manipulation in arctic mesocosms are reproduced by a minimum microbial food web model. Limnol. Oceanogr. **60**: 360–374. doi:10.1002/lno.10025

Le Quéré, C. and others 2016. Role of zooplankton dynamics for southern ocean phytoplankton biomass and global biogeochemical cycles. Biogeosciences **13**: 4111–4133. doi:10.5194/bg-13-4111-2016

Leblanc, K. and others 2012. A global diatom database - abundance, biovolume and biomass in the world ocean. Earth Syst. Sci. Data **4**: 149–165. doi:10.5194/essd-4-149-2012

Litchman, E., C. A. Klausmeier, O. M. Schofield, and P. G. Falkowski. 2007. The role of functional traits and trade-offs in structuring phytoplankton communities: Scaling from cellular to ecosystem level. Ecol. Lett. **10**: 1170–1181. doi:10.1111/j.1461-0248.2007.01117.x

Litchman, E., and C. A. Klausmeier. 2008. Trait-based community ecology of phytoplankton. Annu. Rev. Ecol. Evol. Syst. **39**: 615–639. doi:10.1146/annurev.ecolsys.39.110707.173549

Litchman, E., M. D. Ohman, and T. Kiørboe. 2013. Trait-based approaches to zooplankton communities. J. Plankton Res. **35**: 473–484. doi:10.1093/plankt/fbt019

Löptien, U., and H. Dietze. 2015. Constraining parameters in marine pelagic ecosystem models - is it actually feasible with typical observations of standing stocks? Ocean Sci. **11**: 573–590. doi:10.5194/os-11-573-2015

Luo, Y. W. and others 2012. Database of diazotrophs in global ocean: Abundance, biomass and nitrogen fixation rates. Earth Syst. Sci. Data **4**: 47–73. doi:10.5194/essd-4-47-2012

Mariani, P., K. H. Andersen, A. W. Visser, A. D. Barton, and T. Kiørboe. 2013. Control of plankton seasonal succession by adaptive grazing. Limnol. Oceanogr. **58**.

Marki, A., and M. Pahlow. 2016. Microzooplankton stoichiometric plasticity inferred from modeling mesocosm experiments in the Peruvian upwelling region. Front. Mar. Sci. **3**: 258. doi:10.3389/fmars.2016.00258

Mitra, A. and others 2014*a*. Bridging the gap between marine biogeochemical and fisheries sciences; configuring the zooplankton link. Prog. Oceanogr. **129**: 176–199. doi:10.1016/j.pocean.2014.04.025

Mitra, A. and others 2014*b*. The role of mixotrophic protists in the biological carbon pump. Biogeosciences **11**: 995–1005. doi:10.5194/bg-11-995-2014

Mitra, A. and others 2016. Defining planktonic protist functional groups on mechanisms for energy and nutrient acquisition: Incorporation of diverse mixotrophic strategies. Protist **167**: 106–120. doi:10.1016/j.protis.2016.01.003

Moriarty, R., and T. O'Brien. 2013. Distribution of mesozooplankton biomass in the global ocean. Earth Syst. Sci. Data **4**: 45–55. doi:10.5194/essd-5-45-2013

O'Brien, C. J. and others 2013. Global marine plankton functional type biomass distributions: Coccolithophores. Earth Syst. Sci. Data **5**: 259–276. doi:10.5194/essd-5-259-2013

Odate, K. 1994. Zooplankton biomass and its long-term variation in the western North Pacific Ocean, Tohoku Sea area, Japan. Bull. Tohoku Natl. Fish. Res. Inst. **56**: 115–173.

Ohman, M. D., and J.-B. Romagnan. 2016. Nonlinear effects of body size and optical attenuation on diel vertical migration by zooplankton. Limnol. Oceanogr. **61**: 765–770. doi:10.1002/lno.10251

Paffenhöfer, G.-A. 1993. On the ecology of marine cyclopoid copepods (Crustacea, Copepoda). J. Plankton Res. **15**: 37–55. doi:10.1093/plankt/15.1.37

Pahlow, M., and A. E. F. Prowe. 2010. Model of optimal current feeding in zooplankton. Mar. Ecol. Prog. Ser. **403**: 129–144. doi:10.3354/meps08466

Prowe, A. E. F., M. Pahlow, S. Dutkiewicz, M. Follows, and A. Oschlies. 2012*a*. Top-down control of marine phytoplankton diversity in a global ecosystem model. Prog. Oceanogr. **101**: 1–13. doi:10.1016/j.pocean.2011.11.016

Prowe, A. E. F., M. Pahlow, and A. Oschlies. 2012*b*. Controls of the diversity-productivity relationship in a marine ecosystem model. Ecol. Model. **225**: 167–176. doi:10.1016/j.ecolmodel.2011.11.018

Rose, J. M., and D. A. Caron. 2007. Does low temperature constrain the growth rates of heterotrophic protists? Evidence and implications for algal blooms in cold waters. Limnol. Oceanogr. **52**: 886–895. doi:10.4319/lo.2007.52.2.0886

Ryther, J. H. 1969. Photosynthesis and fish production in the sea. Science **166**: 72–76. doi:10.1126/science.166.3901.72

Saba, V. S. and others 2011. An evaluation of ocean color model estimates of marine primary productivity in coastal and pelagic regions across the globe. Biogeosciences **8**: 489–503. doi:10.5194/bg-8-489-2011

Sailley, S. F. and others 2013. Comparing food web structures and dynamics across a suite of global marine ecosystem models. Ecol. Model. **261–262**: 43–57. doi:10.1016/j.ecolmodel.2013.04.006

Sailley, S. F., L. Polimene, A. Mitra, A. Atkinson, and J. I. Allen. 2015. Impact of zooplankton food selectivity on plankton dynamics and nutrient cycling. J. Plankton Res. **37**: 519–529. doi:10.1093/plankt/fbv020

San Martin, E., R. P. Harris, and X. Irigoien. 2006. Latitudinal variation in plankton size spectra in the Atlantic Ocean. Deep-Sea Res. Part II Top. Stud. Oceanogr. **53**: 1560–1572. doi:10.1016/j.dsr2.2006.05.006

Schmoker, C., S. Hernandez-Leon, and A. Calbet. 2013. Microzooplankton grazing in the oceans: Impacts, data variability, knowledge gaps and future directions. J. Plankton Res. **35**: 691–706. doi:10.1093/plankt/fbt023

Smith, S. L., M. Pahlow, A. Merico, and K. W. Wirtz. 2011. Optimality-based modeling of planktonic organisms. Limnol. Oceanogr. **56**: 2080–2094. doi:10.4319/lo.2011.56.6.2080

Smith, S. L., A. Merico, K. W. Wirtz, and M. Pahlow. 2014. Leaving misleading legacies behind in plankton ecosystem modelling. J. Plankton Res. **36**: 613–620. doi:10.1093/plankt/fbu011

Steinberg, D. K., and M. R. Landry. 2017. Zooplankton and the ocean carbon cycle. Ann. Rev. Mar. Sci. **9**: 413–444. doi:10.1146/annurev-marine-010814-015924

Stock, C. A., J. P. Dunne, and J. G. John. 2014*a*. Drivers of trophic amplification of ocean productivity trends in a changing climate. Biogeosciences **11**: 7125–7135. doi:10.5194/bg-11-7125-2014

Stock, C. A., J. P. Dunne, and J. G. John. 2014*b*. Global-scale carbon and energy flows through the marine planktonic food web: An analysis with a coupled physical-biological model. Prog. Oceanogr. **120**: 1–28. doi:10.1016/j.pocean.2013.07.001

Stock, C. A. and others 2017. Reconciling fisheries catch and ocean productivity. Proc. Natl. Acad. Sci. USA **114**: E1441–E1449. doi:10.1073/pnas.1610238114

Su, B., M. Pahlow, and A. E. F. Prowe. 2018. The role of microzooplankton trophic interactions in modelling a suite of mesocosm ecosystems. Ecol. Model. **368**: 169–179. doi:10.1016/j.ecolmodel.2017.11.013

Turner, J. T. 2004. The importance of small planktonic copepods and their roles in pelagic marine food webs. Zool. Stud. **43**: 255–266.

Uitz, J., H. Claustre, B. Gentili, and D. Stramski. 2010. Phytoplankton class-specific primary production in the world's oceans: Seasonal and interannual variability from satellite observations. Global Biogeochem. Cycles **24**: GB3016. doi:10.1029/2009GB0036830

Visser, A. W. 2007. Motility of zooplankton: Fitness, foraging and predation. J. Plankton Res. **29**: 447–461. doi:10.1093/plankt/fbm029

Visser, A. W., and O. Fiksen. 2013. Optimal foraging in marine ecosystem models: Selectivity, profitability and switching. Mar. Ecol. Prog. Ser. **473**: 91–101. doi:10.3354/meps10079

Vogt, M. and others 2012. Global marine plankton functional type biomass distributions: *Phaeocystis* spp. Earth Syst. Sci. Data **4**: 107–120. doi:10.5194/essd-4-107-2012

Ward, B. A., S. Dutkiewicz, A. D. Barton, and M. J. Follows. 2011. Biophysical aspects of resource acquisition and competition in algal mixotrophs. Am. Nat. **178**: 98–112. doi:10.1086/660284

Ward, B. A., S. Dutkiewicz, O. Jahn, and M. J. Follows. 2012. A size-structured food-web model for the global ocean. Limnol. Oceanogr. **57**: 1877–1891. doi:10.4319/lo.2012.57.6.1877

Ward, B. A., S. Dutkiewicz, and M. J. Follows. 2013. Modelling spatial and temporal patterns in size-structured marine plankton communities: Top-down and bottom-up controls. J. Plankton Res. **36**: 31–47. doi:10.1093/plankt/fbt097

Ward, B. A., and M. J. Follows. 2016. Marine mixotrophy increases trophic transfer efficiency, mean organism size, and vertical carbon flux. Proc. Natl. Acad. Sci. USA **113**: 2958–2963. doi:10.1073/pnas.1517118113

Wunsch, C., and P. Heimbach. 2007. Practical global oceanic state estimation. Physica D **230**: 197–208. doi:10.1016/j.physd.2006.09.040

Zamora-Terol, S., T. G. Nielsen, and E. Saiz. 2013. Plankton community structure and role of *Oithona similis* on the western coast of Greenland during the winter-spring transition. Mar. Ecol. Prog. Ser. **483**: 85–102. doi:10.3354/meps10288

Acknowledgments

We are very grateful to Stephanie Dutkiewicz and Iris Kriest for insightful comments during the development of this manuscript and to Philipp Brun for setting up the statistical analysis. We would also like to thank two anonymous reviewers for constructive comments improving the manuscript. This work contributes to the Priority Programm 1704—Dynatrait funded by the German Research Foundation. The Centre for Ocean Life is a VKR Centre of Excellence funded by the Villum Foundation. We acknowledge the use of data from the Odate collection owned by the Tohoku National Fisheries Research Institute and supported by the Global Environmental Research Fund of the Japanese Ministry of the Environment. The SO-CPR Survey supported by the Scientific Committee on Antarctic Research (SCAR) and the COPEPOD database of the National Oceanic and Atmospheric Administration (NOAA).

Conflict of Interest

None declared.

Submitted 19 March 2018
Revised 22 August 2018
Accepted 03 October 2018

Associate editor: Thomas Anderson